Digest Journal of Nanomaterials and Biostructures Vol. 20, No. 4, October-December 2025, p. 1639-1663

Numerical modeling of a PDMS-based microfluidic channel for precision drug delivery system

T. Archana [a,b*], N. Nachammai [a], S. Praveen Kumar [b], S. Kumaran [c]
[a] *Department of Electronics and Instrumentation Engineering, Annamalai University, Chidambaram, Tamil Nadu- 608002.India.*
[b] *Department of Electronics and Communication Engineering, Saveetha Engineering College, Thandalam, Chennai- 602105.*
[c] *Department of Electronics and Communication Engineering, Saveetha School of Engineering, Saveetha Institute of Medical and Technical Sciences (SIMATS), Chennai, India. 602 105.*

Polydimethylsiloxane (PDMS) is a biodegradable polymer-based silicone elastomer material often widely used in microfluidic channels to enhance the controlled drug delivery flow rate. The preclinical models of inefficiency in screening drugs for predicting clinical outcomes could be replaced by microfluidic platforms, which have the potential to offer a faster and more economical alternative. However, achieving such an intricately managed administration of a pharmaceutical compound is not a simple task and continues to present a significant challenge. The current study put forward various microchannels with modified configurations to decrease the rate at which drugs are released, enhance pH responsiveness with high precision in drug delivery, and establish a specific order of sequence. The potential modifications in microfluidic and micro-reservoir design include linearity, increasing resistor connection, dimensions, and sizes. Incorporating an analogous electrical circuit in microfluidic systems facilitates a more suitable approach to their design and analysis. The results indicate that designed microchannels can control the decreased release rate of the model. The proposed microfluidic design accuracy is validated by computational analysis.

(Received September 29, 2025; Accepted December 28, 2025)

Keywords: Polydimethylsiloxane, microfluidic channel, Electrical resistors, Finite Element Analysis, Drug delivery.

1. Introduction

The increasing demand for environmentally friendly and high-performance energy storage Polydimethylsiloxane (PDMS) is a functional synthetic material for improving optical performance [1], microchannels of drug realizing rate [2, 3], clinical [4], and renewable energy of triboelectric nanogenerators (TENG) [5] due to recoverable Yong's modulus, high porous, increasing hydrophobic properties, and non-toxic behavior, and oxygen permeable [6]. The manufacturing cost of PDMS material is significantly lower than glass and silicon wafers. Moreover, its light transmittance, favorable biocompatibility, and capacity to readily adhere to various materials at ambient temperature have received more attraction. PMMA and PTGE are the predominant elastomeric materials employed in manufacturing microfluidic devices using solid lithography techniques [7, [8]. The major drawback of this two-elastomer material is its susceptibility to enlargement when disclosed with an excessive amount of acetone as a solvent. The enlargement influences the release rate of fluid and the generation of uncontrolled transports in microchannels [9]. PDMS and cyclic olefin copolymer (COC) are alternative polymers

* Corresponding author: archathiru2712@gmail.com
https://doi.org/10.15251/DJNB.2025.204.1639

demonstrating chemical resistance against powerful solvents. These particular polymers are employed in the production of microfluidic devices through the utilization of the hot-embossing technique [10].

Novel approaches to enhancing drug delivery and the development of novel technologies for well-coordinated transmission yield superior therapeutic outcomes by optimizing the bioavailability and therapeutic efficacy of medicinal agents, thereby concomitantly mitigating undesirable adverse reactions. The ordinary drug delivery system is affected by several factors, such as non-uniform dispersed molecules affecting the release rate utilization of a high percentage of drugs/chemicals. The limitations in this field are posed by the constraints associated with the production of carriers that contain multiple therapeutic agents, as well as the challenges of achieving localized drug delivery and studying the therapeutic and toxic effects [11, 12].

A microfluidic device comprises numerous branches of drug delivery, encompassing biotechnology, biological science, and engineering [13]. The domain of microfluidic drug delivery channels and their corresponding design modifications has mobilized significant attention over the past decade in therapeutic interventions. The requirement for modifications in design is linked to the field of science that deals with producing microfluidic channels and reservoirs to regulate the characteristics of fluid flow in small quantities, whose sizes range from 10 to 100 micrometers [14]. The microfluid device is used as a different technology that was recognized with a wide range of applications such as energy [15], biological chemistry [16], atmospheric sensing [17], therapeutic diagnostics [18], micro-propulsion [19], and drug delivery [20]. Microfluidics produces nanoparticles with required particle size (P.S.) and low polydispersity indices (PDIs). Hazardous substances in microfluidics can be used without disclosure to carcinogenic samples, ensuring safety. Microfluidic devices do not demand extensive industrial areas and assure consistent replication from one batch to another [21].

Sequential drug delivery is associated with two or more drugs with multiple mechanisms of action and produced in a fixed order, which can obtain synergetic efficiency due to the optimized sequential action mode. It can avoid drug interaction (DDI) during simultaneous drug delivery [22]. The methodology involves gradually distributing various medications through sequential administration via the parenteral pathways or utilizing controlled-release drug delivery mechanisms. The drug delivery system can be performed with different technologies, such as double coating [23], pursuing hybrid materials [24], and biodegradable polymers [25]. Despite this, they have yet to deliver the needed accuracy or robustness in regulating the time variations of discharge activation. Therefore, there is a desire to regulate the "time at which release is activated", particularly for drug delivery systems that are passive to administer one or more drugs sequentially.

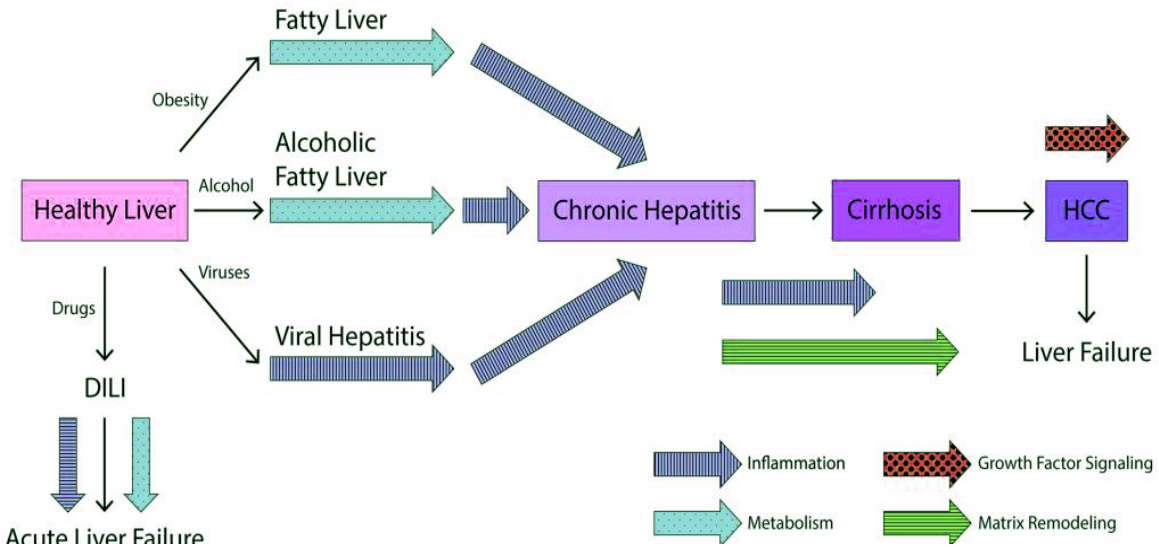

Fig. 1. Illustrates the regenerative mechanism involved in the pathogenesis of liver disease [26].

Liver diseases are responsible for over 800 million cases and result in approximately 2 million deaths annually on a global scale [27, 28]. The increased morbidity associated with liver diseases can be attributed not only to the high prevalence of liver-specific insults such as viral infections and drug misuse, but also to the growing population affected by metabolic syndromes. The mortality rate of liver diseases is predominantly associated with advanced stage conditions, such as hepatocellular carcinoma (HCC) and cirrhosis, both of which tend to develop gradually over time [29]. The liver's complex structure and functions, which include synthesis, metabolism, and disposal, are exemplified by the existence of repeated lobules at the cellular level and its role in preserving blood homeostasis. As such, delivering medicinal drugs to the liver is an extremely difficult task with several challenges. Foreign agents identified within the hepatic cells undergo rapid conversion or metabolism, resulting in their conversion into a non-toxic state and subsequent loss of their original characteristics [30]. Progress in innovative drug delivery systems has enhanced the pharmacodynamics of therapeutic agents, such as small molecules and peptide drugs, to tackle the difficulties linked to their administration [31]. Consequently, these improvements have led to heightened effectiveness and diminished hepatotoxicity.

The present investigation proposes the microfluidic channel to control the drug realizing rate, sequential drug delivery, and responsiveness to the atmospheric conditions by implementing a reservoir-microfluidic channel. The diffusive carrier of molecules through channels is contingent upon the channel's geometry, specifically its length and cross-sectional area, as per Fick's law and the existing concentration gradient. Zero-order delivery is possible since the reservoir's medication concentration is still over the solubility limit. Changing the length of the channel allows the required drug release rate. The reservoir unit within the microfluidic channel can be identified by its diverse geometric configurations connected to the electrical circuitry, including components such as capacitors and resistors. Microchannels were infused with biodegradable polymers, which underwent hydrolysis degradation, resulting in the channels opening after a certain period. This approach was employed to effectively regulate the initiation of drug delivery or enable sequential delivery from considerable reservoirs. Moreover, it was determined that micro-channels have the intrinsic ability to regulate the dispensation of medicinal substances that possess solubility dependent on pH by the pH level of the surrounding channel environment.

2. Experimental section

2.1. Materials

PDMS and Methylene blue (MB) both materials are received from Sigma-Aldrich® Solutions in Chennai. The material properties of MB are shown in Table 1.

Table 1 Parameters used for drug delivery analysis.

Material	Parameters	Value
Methylene Blue	Molecular Weight, Mw	319.85 g/mol
	Solubility Limit	125.06 mol/m3
	Diffusion Coefficient	7.6 × 10-10 m2/s

2.2 Governing Equations for drug release rate

A drug release rate is controlled by an elementary unit that can control the drug initiation based on the straight microfluidic channels and reservoir. The drug release-controlled factors, such

as length of channels, cross-sectional area, and two or more channels, were systematically modified to assess their impact on the rates at which pharmaceutical substances are discharged. The M.B. release rate is calculated from each microfluidic device per Fick's law using a diffusion coefficient of 7.6x10-6 m2/s.

The force applied on the P.S. can be written as

$$F_r = -\nabla V(r) \quad (1)$$

Thus, the diffusion coefficient depends on the molecule's dimensions and configuration, its interaction with the surrounding solvent, and the solvent's viscosity.

$$D = \frac{k_b T}{f}[f - Frictional\ coefficient]\ [f = 6\pi\eta r] \quad (2)$$

$D = \frac{k_b T}{6\pi\eta r}$ [kb-Boltzmann constant, r-radius diffusing sphere, η-viscosity of fluid] (3)

Fick's law associated with the Navier-stroke equation for mass transfer is observed much faster than diffusion based on the all-simple channels due to the viscous fluid flow. The basic flow of channels arises from the stochastic movements of atoms influenced by a distinct driving force, exemplified by a pressure gradient, which yields comparable rates. The dissimilarities between the solid states and liquid states arise due to the occurrence of self-diffusion, which is facilitated by exchanges of atoms and vacancies. Consequently, this type of diffusion can induce alterations in shape and the movement of particles within the solid phase.

Furthermore, if an atom possesses a gradient in its chemical potential, it proceeds to advance towards neighboring atoms per the innovative concept introduced by Fick's first law.

The velocity of molecule in the x-direction in fluid flow as

$$u_x + a\frac{\partial u_x}{\partial x} + \frac{a^2}{2}\frac{\partial^2 u_x}{\partial x^2} \quad (4)$$

Where 'a' is the distance from the first peak intensity radial distribution function

Conversely, the velocity of the molecule reversed motion as

$$u_x - a\frac{\partial u_x}{\partial x} + \frac{a^2}{2}\frac{\partial^2 u_x}{\partial x^2} \quad (6)$$

Therefore, $\frac{\partial \mu_x}{\partial x}$, $-a\frac{\partial \mu_x}{\partial x}$ Is the velocity difference between the molecules and the average velocity of closer to two neighbour molecules can be expressed as follows

$$u_x + \frac{a^2}{2}\frac{\partial^2 u_x}{\partial x^2} \quad (7)$$

The relative velocity of neighbor atoms in 'x' direction

$$u_x - u_x + \frac{a^2}{2}\frac{\partial^2 u_x}{\partial x^2} \quad (8)$$

There might be a motive for the diffusion process, such as the presence of a chemical potential gradient. $\frac{\partial \mu_x}{\partial x}$, the relative velocity of molecules concerning the Fick's law

$$\frac{a^2}{2}\frac{\partial^2 u_x}{\partial x^2} = \frac{D}{RT}\frac{\partial \mu}{\partial x} \quad (9)$$

For mass transfer concerning the mass concentration of particles linked to the Ficks law diffusive mass heat flux i(∂m_i), according to the Ficks law

$$\partial m_i = -\rho D_{i,m}\frac{\partial m_i f_i}{\partial x} = -D_{i,m}\frac{\partial c_i}{\partial x} \quad (10)$$

2.3. Boundary conditions

The diffusive transmission formulation for a single straight channel can be written as follows.

$$\frac{\partial(p\emptyset)}{\partial t} = \nabla.(\rho D_c \nabla\emptyset) + S_\emptyset \quad (\phi = c/p)$$

$$\frac{\partial c}{\partial t} = \nabla.(D_c \nabla_c) + S_{c/p} \quad (12)$$

Where ρ-density, Sc/p = volumetric source, Dc-kinematic diffusivity, is a conserved quantity.

The model's laminar nature also leads to the absence of an energy equation. The water is fixed as a fluid medium. The properties of drug materials are density = 998.2 kg/m3, viscosity, μ = 1x10-3, diffusion coefficient (D) = 7.6x10-6 m2/s.

The diffusion analysis conducted at the upper part of the reservoir led to the formation of a logarithmic diffusion form for the inlet boundary condition. This diffusion form was generated through the variation of pH value over time. The assumed attributes of the drug align with those observed at a temperature of 27 °C. There is a no-slip wall condition used for fluid-solid interaction.

2.4. Computational analysis

The drug was administered into the reservoirs using PDMS micro stamps. The PDMS stamp was made by pouring PDMS into an aluminum mold, which produced many micropillars that varied in size from 800 µm to 1 mm. Fig. 2 shows the proposed model design with different microfluidic elementary channel device. Drug inks were formulated by combining model drugs in distilled water until they reached their maximum solubility. A singular printing included an average drug loading of 3 ± 0.5 µg. The design parameters and various geometrical factors of microfluidic unit is shown in Table 2.

Table 2 Design parameters for geometric factors of the microfluidic unit.

Design	Elementary Unit	Parameters	Dimensions
Microfluidic elementary device	Drug Reservoir	Width x Length x Height	1 mm x1 mm x 20 µm
	Micro Channel	Width x Length x Height	20 µm x 1 mm x 20 µm
	Capacitance	Width x Length Height	200 µm x 200 µm 20 µm

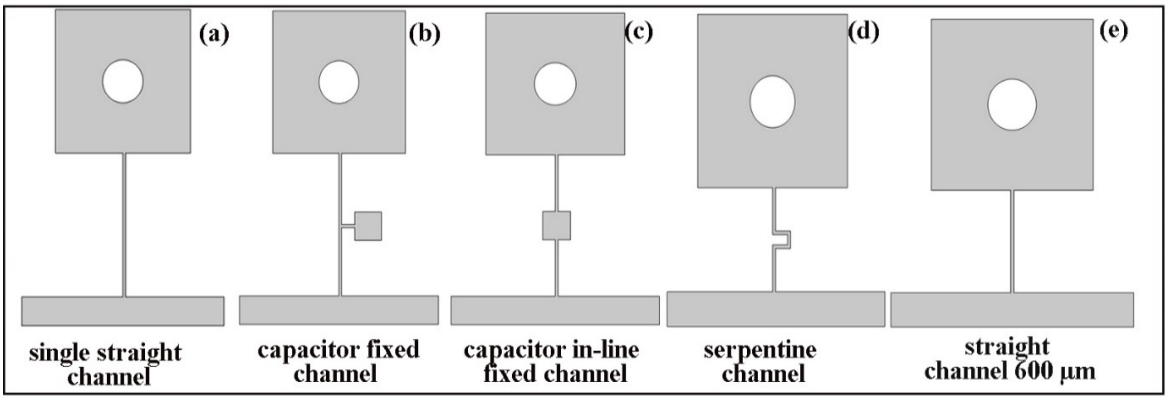

Fig. 2. Microfluidic channel design (a) Single channel with straight channel (b) straight with side capacitor fixed channel (c) straight with side in-line capacitor fixed channel (d) serpentine channel (e) straight channel short length (600 µm).

2.5. Validation

The proposed design of the microfluidic device is validated by steady-state and transient conditions such as pressure delivery and velocity profile. The streamlined flows and contour diagram show the diffusion effect of microfluidic channels, velocity difference, and particle delivery time concerning the uniform flow field. It is well accepted that non-uniform diffusion

characteristics are exceedingly unfavorable and that the existence of flow route heterogeneities can cause the appearance of inactive diffusion flow.

Through a mesh-independence analysis, a thorough examination was conducted to establish the adequacy of the element utilized in representing the solid and fluid domains—convergence criteria for the fluid domain encompassing maximum pressure and velocity utilization. The attainment of converged results was accomplished upon observing changes in those solutions that fell below a threshold of 5%.

2.6. Statistical analysis

An optimization technique Response Surface Methodology (RSM) was employed, utilizing a box Benkhan design, to determine the ideal geometrical parameters of PDMS based microfluidic device. The study focused on evaluating the impact of three independent variables, namely the Number of channels (A) and the channel width (B) and channel length (C) on drug release rate. The design included three levels of each of the three components, resulting in the 18 trials that are shown in Table 3.

Table 3 Microfluidic geometrical factors and levels.

S. No	Process parameters	Units	Levels		
			-1	0	1
1	Number of channels	m	1	2	3
2	Channel width	µm	2	5	20
3	Channel length	mm	10	20	30

3. Results and discussion

3.1. Computational analysis of drug release

Computational fluid dynamics studied the controlled drug flow rates using various tool geometry on microchannels. Therefore, to authenticate the impact of capacitor augmentation or tortuosity on the drug liberation conduct, diffusion modelling was conducted employing COMSOL Multiphysics. In Fig 3, a circular area within a drug reservoir in a square was designated as the origin of a representative drug, namely MB. The concentration of MB was adjusted to adhere to the maximum solubility threshold of 4%. The cross-sectional area of each channel is 20 x 20 µm, and the length is 1 mm. The value assigned to the diffusion coefficient of MB is 7.6x10-10 m2/s. As depicted in Fig. 4 and Fig. 5, the straight channel unit typically requires approximately 42 minutes to attain the state of equilibrium following the initiation of the diffusion process.

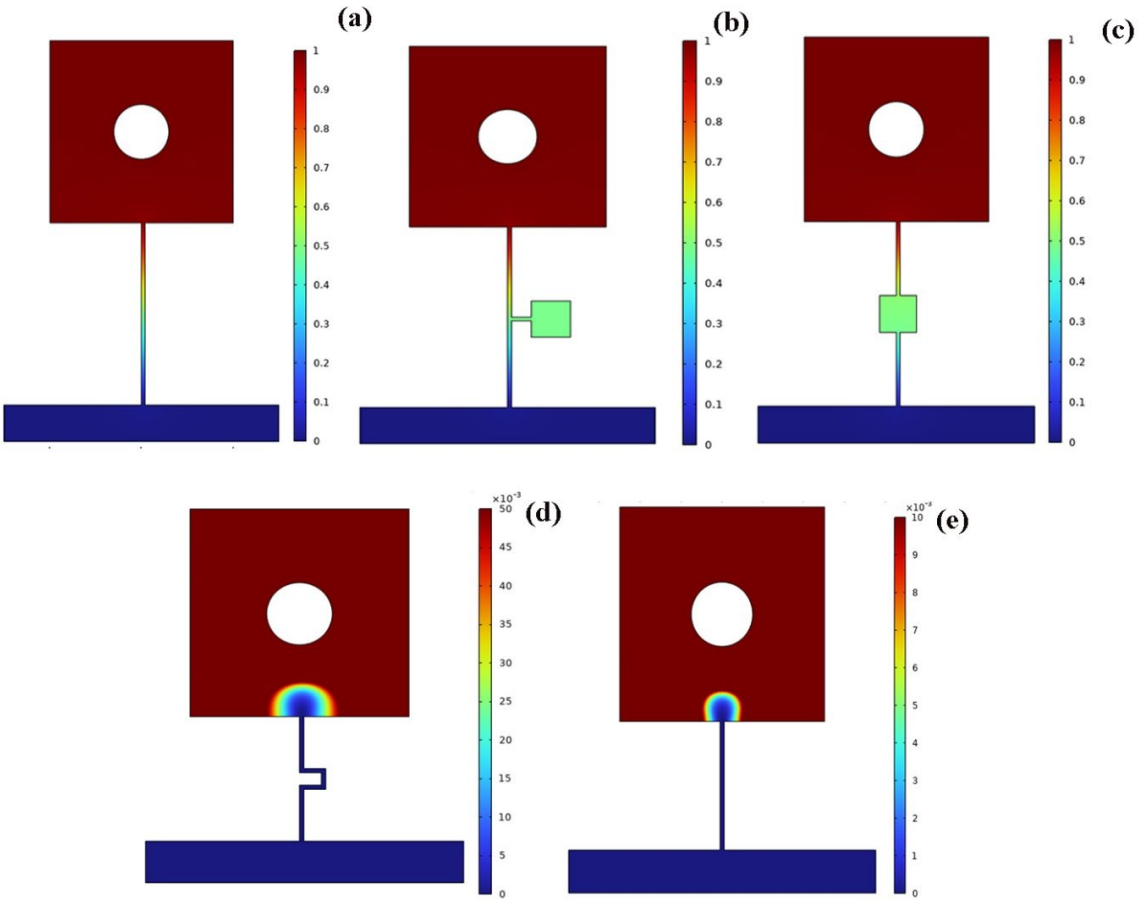

Fig. 3. Diffusion modelling of microfluidic channel system using COMSOL Multiphysics (a) single straight channel (b) side-line capacitor (c) in-line capacitor (d) serpentine (e) 600 µm length channel.

Initially, the tortuosity impact was simulated using a serpentine channel with a beginning-to-end length similar to the linear channel. The release via the serpentine channels was observed to be slower than expected in comparison to the straight channel system. To ascertain the impact of including a capacitor, a rectangular component (referred to as a capacitive element) was introduced into the fundamental channel system, which consisted of a reservoir and a straight channel. Subsequently, the resultant effect was examined and evaluated. The introduction of capacitive components, conversely, extended the duration of the temporary phase as it necessitates a greater amount of time to achieve equilibrium of the supplementary area and attain a stable condition. When a side capacitive element was introduced to the lateral portion of a discharge pathway, it exhibited a delay in attaining its state of equilibrium. However, the system achieved a discharge rate equal to that of the system with a linear discharge pathway once it reached a state of equilibrium.

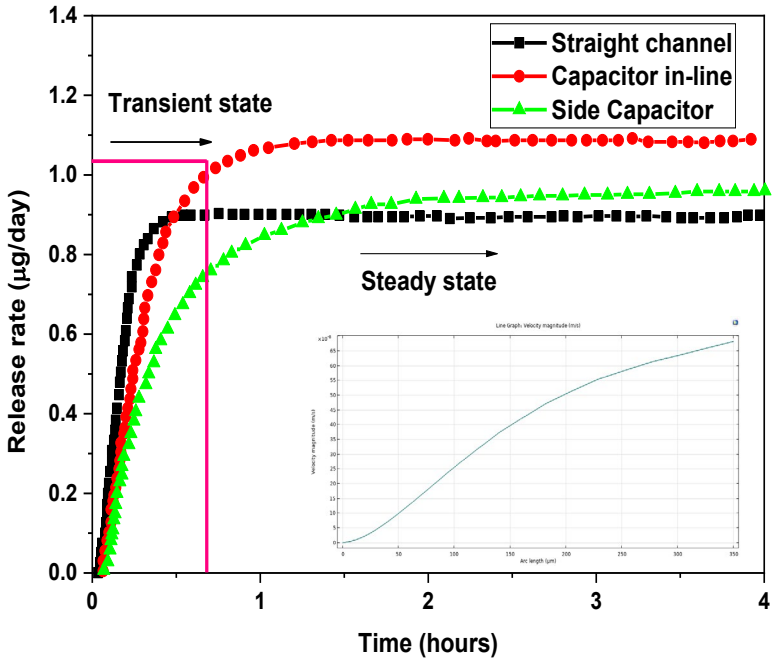

Fig. 4. Modelling of drug release rate for straight channel, capacitor in-line, side capacitor.

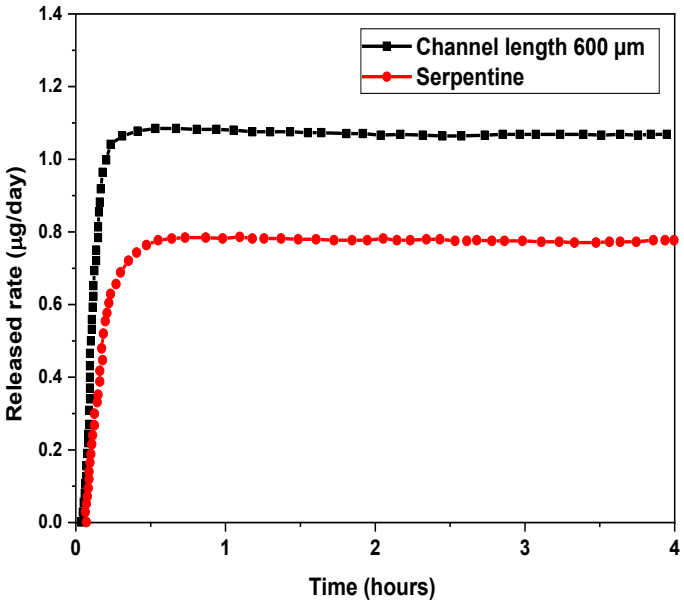

Fig. 5. Modelling of drug release rate for straight channel length 600 µm and serpentine model.

Furthermore, time-dependent transient diffusion analysis with an increasing number of capacitors counts to evaluate the performance of side capacitors throughout the transient state. As a result, the transient state was increased while increasing the capacitor count at the microfluidic channel. A time constant was established to conduct a quantitative analysis of the correlation between the quantity of side capacitors and the duration of the transient condition. The time constant is characterized as the period necessary to accomplish 63.2% of the stable flow. It can be concluded that a longer time constant suggests a gradual state of equilibrium being reached by the system. As demonstrated in Fig 6, the time constant displayed a proportional connection with the

number of capacitors. Hence, one can infer that the quantity of capacitors can proficiently regulate the transient length.

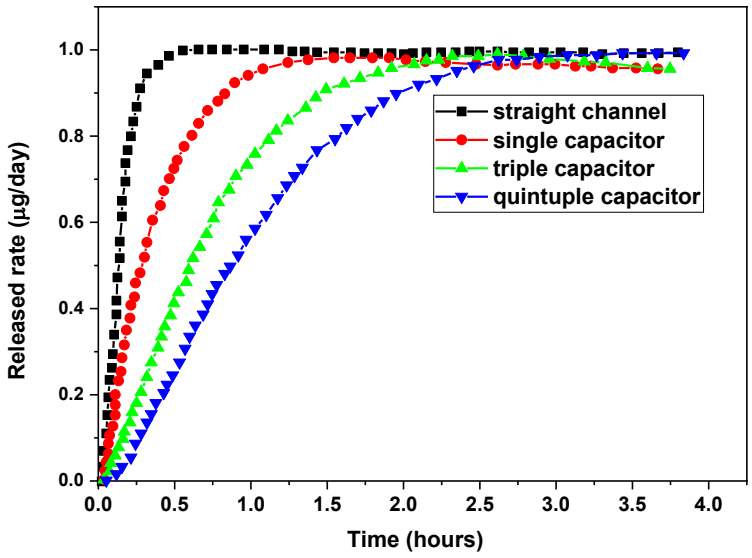

Fig. 6 Modelling of drug release rate single capacitor, triple capacitor, quintuple capacitor.

Devices with channels measuring 2 and 5 µm in width maintained zero-order delivery for the length of the experiment, whereas devices with channels measuring 20 µm in width maintained the zero-order pattern for 24 h. The expedited transportation via channels that are 20 µm wide caused a reduction in the quantity of drugs within the drug reservoir, resulting in a drug concentration that fell below the limit of solubility. As a consequence of this turning point, the difference in concentration between the interior and exterior of the devices gradually decreased, causing a steady decline in drug release from the devices. The estimated and simulated value for various microfluidic channels of drug release rate is shown in Table 4. The modulation of release rates was achieved through the manipulation of channel lengths. The channel lengths of the short, medium and long channels were measured to be 0.7, 1.65, and 3.4 mm, respectively. It was noted that the release rates showed an inverse correlation with the channel lengths. Additionally, there was a rise in the quantity of channels, which led to an expedited release of drugs, displaying a significant association with the number of channels. As a result of their elevated rates of release, devices containing double or triple channels could sustain zero-order delivery for 24 hours. As the breadth and quantity of the channel expanded, it led to a concomitant enlargement of the overall cross-sectional area of the microfluidic elementary device.

Table 4 Calculated and simulated drug delivery (µg/day).

D (m2/s)	S (mol/m3)	A (um2)	L (m)	No of channel	dm/dt (µg/day) with conversion	Simulated drug release rate (µg/day)
Number of channels modified						
7.6x10-10	1.25x102	4x10-10	0.001	1	1.0506	1.52
7.6x10-10	1.25x102	4x10-10	0.001	2	2.1012	1.98
7.6x10-10	1.25x102	4x10-10	0.001	3	3.1519	2.34

Channel width modified.						
7.6x10-10	1.25x102	4x10-12	0.001	1	0.112	0.22
7.6x10-10	1.25x102	2.5x10-11	0.001	1	0.556	0.45
7.6x10-10	1.25x102	4x10-10	0.001	1	1.506	1.56
Channel length modified.						
7.6x10-10	1.25x102	4E-10	0.0007	1	1.5009	1.65
7.6x10-10	1.25x102	4E-10	0.00165	1	0.6367	0.72
7.6x10-10	1.25x102	4E-10	0.0034	1	0.3090	0.46

The impact of tortuosity on the release rate in microchannels was examined through the design of serpentine microchannels, which possessed an equivalent end-to-end distance as the straight channels. As expected, the release rates in the serpentine channels were found to be slower in comparison to the straight channels in Fig 5. The rate of release was increased when a capacitive element also referred to as an in-line capacitor was placed in the middle of a linear route. Because the integrated in-line capacitive design reduced the diffusion resistance in the channel, it functioned as an enlarged section of the route, accelerating the diffusion process, shown in Fig 7 (a-h). However, upon the inclusion of the capacitive component on the periphery of a channel, the discharge rate exhibited a decelerated progress compared to the discharge through a linear channel within the initial eight-hour period. In the following discharge phase, the discharge rate through the capacitor channels poured and reached a level relative to that of the linear channels.

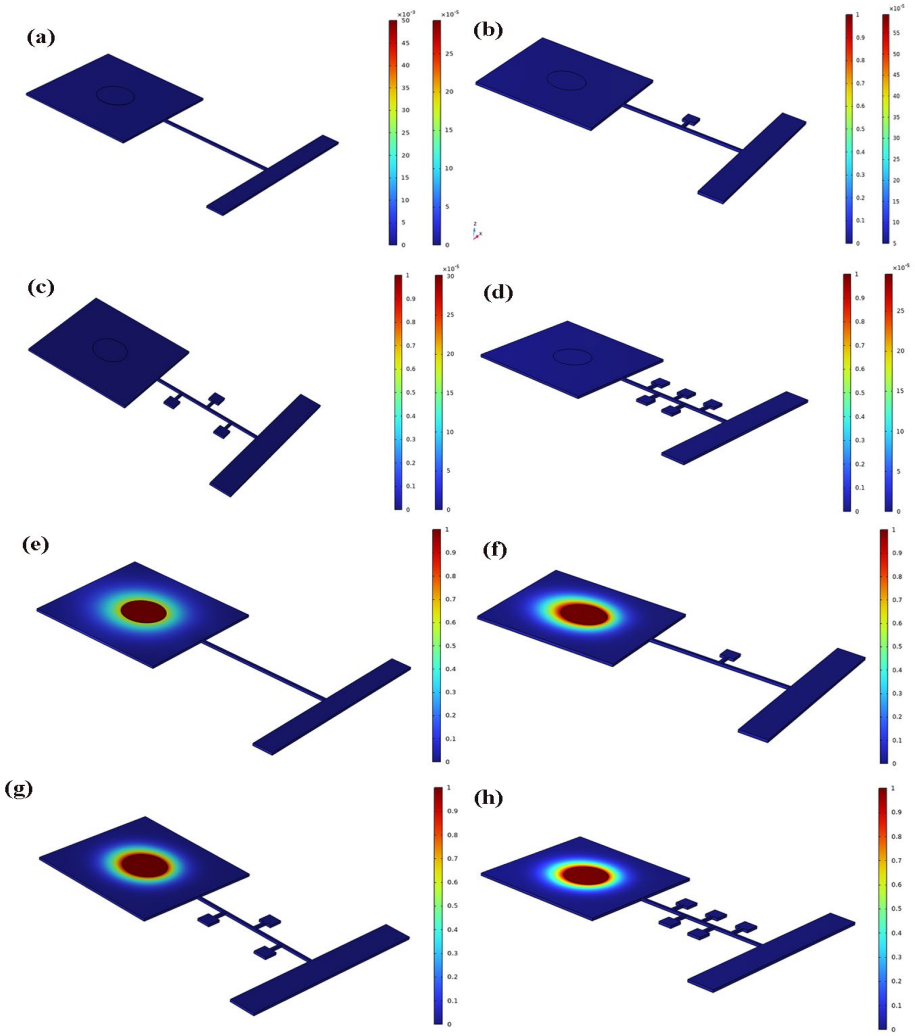

Fig. 7 Volume of diffusive flux (a) straight channel (b) side-line capacitor (c) triple side capacitor (d) Quintuple side capacitor; Surface concentration (e) straight channel (f) side-line capacitor (g) triple side capacitor (h) Quintuple side capacitor.

3.2. Effect of microchannel design

The velocity profile shown in Fig 8 implies that the decelerated diffusion also gives rise to a parabolic curve along the channel length, exhibiting behavior similar to that observed in incompressible and laminar flow within the channel. In spite of being characterized as a molecular or viscous flow, diffusion exhibited similar behaviors to small volume fluid flow in microchannel sizes. Fig 9 shows the graphical depiction of the microchannel's maximum velocity magnitude. The remaining variables stayed the same as those of the microchannel, including the link between pressure and velocity difference in terms of time fluctuations related to the microchannel's designs. During microchannel coordination, the diffusivity is significantly influenced by the microchannel's size. However, since there was no sliding boundary condition, wall slip velocity was almost nil. Compared to the channel's middle, the slip velocity at the wall was noticeably lower.

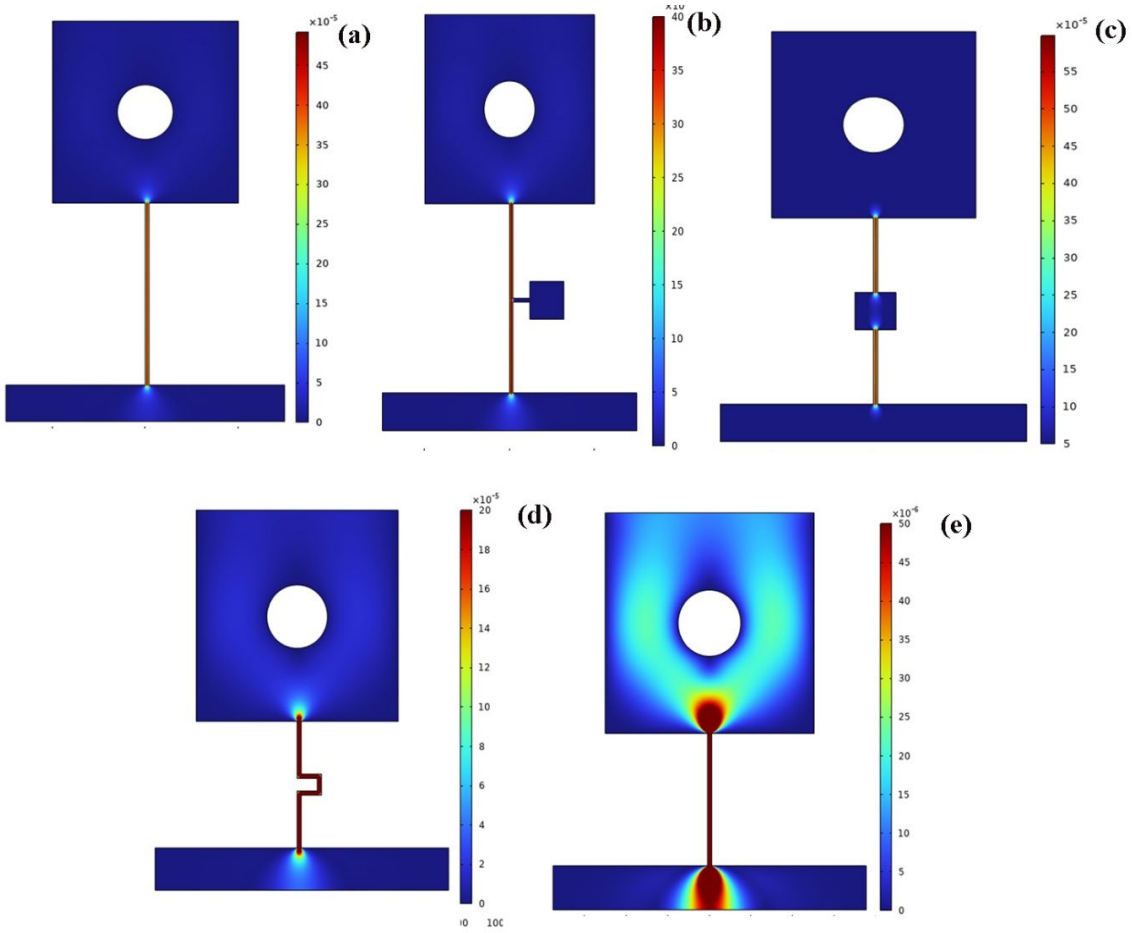

Fig. 8 Effect of microfluidic channel on velocity profile (a) Straight microchannel (b) straight with in-line capacitor (c) straight with side line capacitor (d) serpentine channel.

Fig 9 (a–d) displays the flow velocity distribution along the horizontal center line, y (m), of the channel section for all microchannel sizes. Fig 10 and 11, demonstrate the comparison of simulation results about the diffusion rate at 1 and 20 seconds for each microchannel. It was observed that the diffusion rate increased with the enlargement of the microchannel size, which aligns with the previously anticipated behavior described by diffusion equation no 1. Moreover, the variations in diffusion rate exhibited a linear decrease concerning time over 20 seconds.

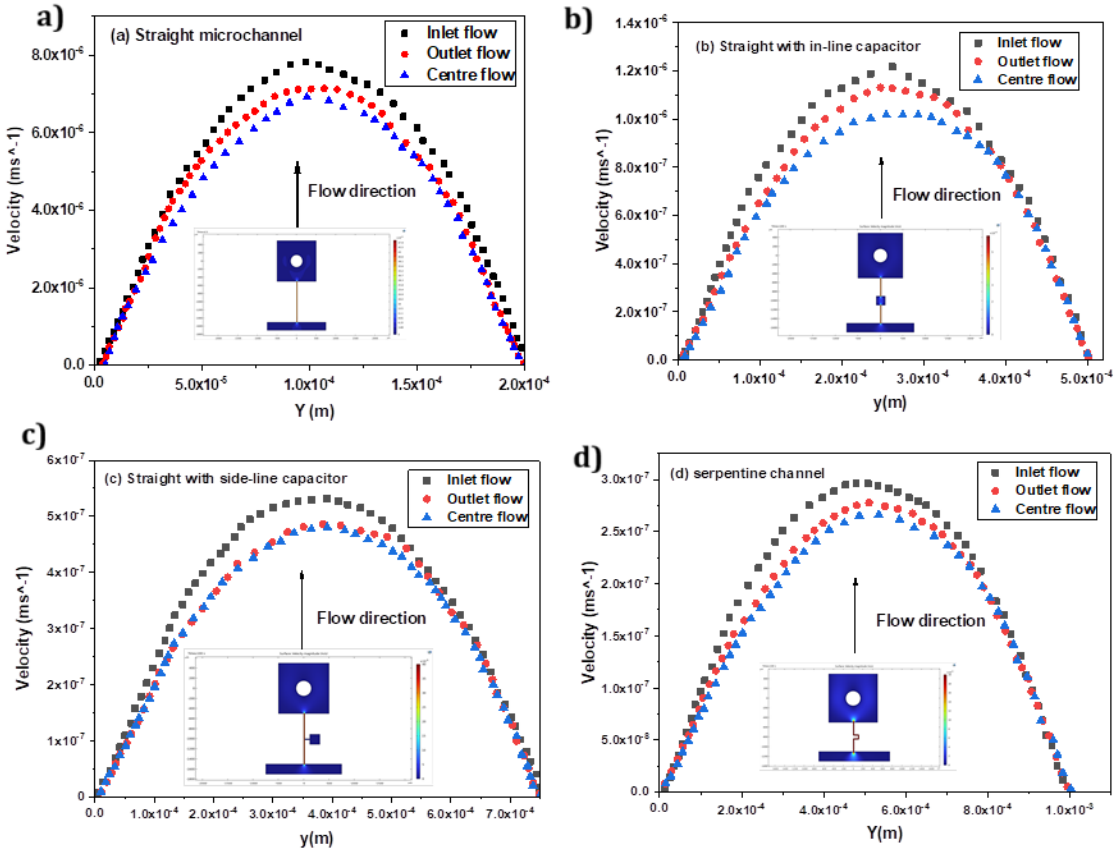

Fig. 9 Effect of microfluidic channel on velocity profile (a) Straight microchannel (b) straight with in-line capacitor (c) straight with side line capacitor (d) serpentine channel.

It was noted that the pressure difference and velocity difference underwent proportional increases or decreases by the microchannel size, as depicted in Figures 10 and 11, due to the substantial disparity in the cross-sectional area and capacitor addition of the channels compared to the straight microchannel. The outcomes derived from the investigation into diffusion rate across microchannels of varying sizes consistently conformed to the fundamental principles outlined in the equation governing diffusion.

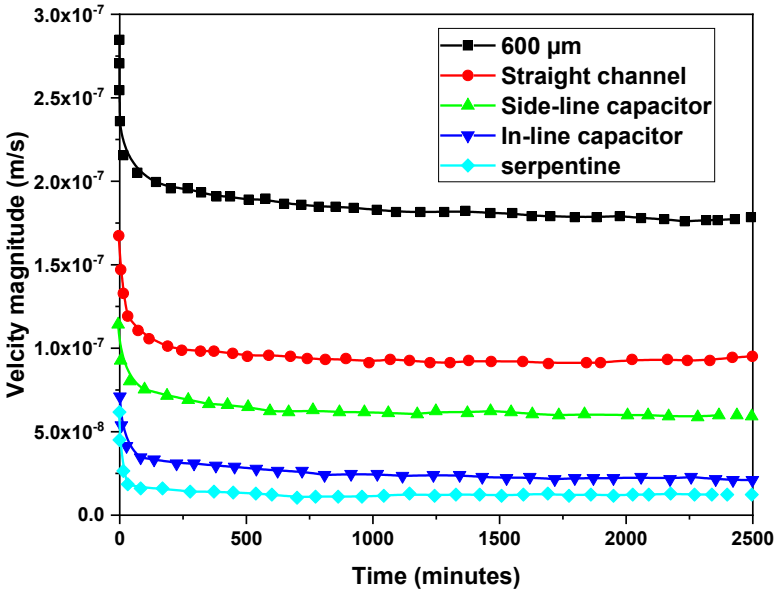

Fig. 10 Velocity magnitude for various microchannel design configurations.

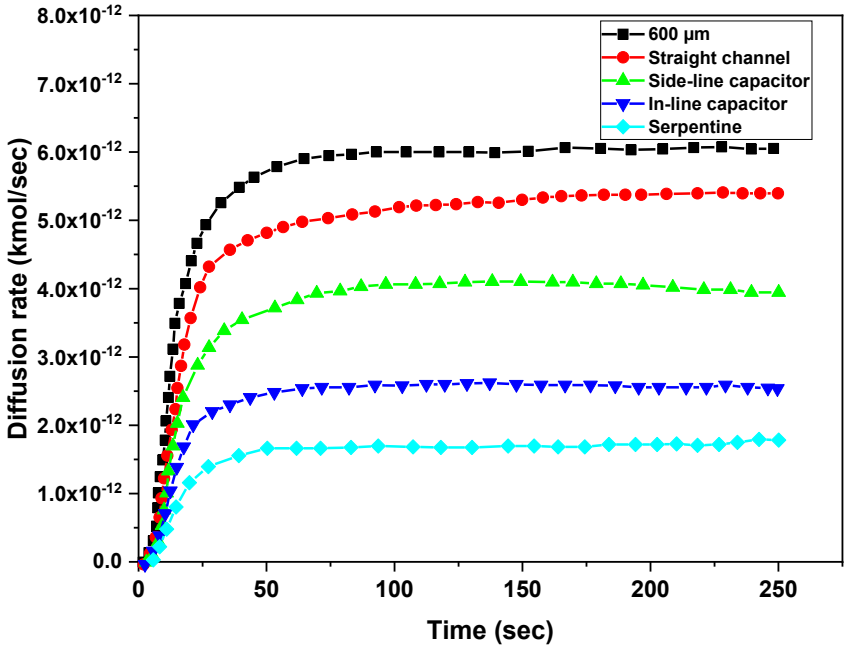

Fig. 11 Simulation result of diffusion rate for different microchannel configurations.

3.3. Sequential drug delivery

A microfluidic device including release channels filled with biodegradable polymer was developed to control the length of medication release. This particular polymer that can decompose naturally impedes the penetration of water into the apparatus until it deteriorates, and prolongs the process of the drug dissolving in the storage area. The initiation of drug release can be adjusted by choosing a biodegradable polymer that possesses varying rates of degradation. In this research endeavor, the utilization of a biodegradable polymer known as poly (DL-lactide-coglycolide), which undergoes degradation within a short span of time, was employed. As depicted in Fig 13,

the initiation of MB liberation occurred promptly for devices lacking any form of delaying mechanism.

In contrast, the commencement of MB liberation from devices equipped with a delaying mechanism was only fully realized after three days. Over three days, the biodegradable polymer that was present in the microchannels underwent a gradual process of degradation, which subsequently resulted in the creation of a pathway for the ingress of water molecules. This observation implies the potential for regulating the duration of delay by considering the extent of filling and the rate of material degradation in the release channels. The rate of release (also known as the slope) from the devices incorporating the delaying mechanism exhibited a slightly reduced pace compared to the control devices. This phenomenon can be attributed to residual portions of PDMS within the release channels during the degradation process, which hindered the diffusion of MB.

Table 5 Calculated and simulated drug delivery (µg/day).

Number of channels	D (m2/s)	S (mol/m3)	A (um2)	L (m)	dm/dt (µg/day) with conversion	Sequential delivery (µg/day)	Simulated drug release rate (µg/day)
Single	7.6x10-10	1.25x10+02	4x10-10	0.001	1.05	1.46	1.52
Double	7.6x10-10	1.25x10+02	4x10-10	0.001	2.10	1.82	1.98
Tripple	7.6x10-10	1.25x10+02	4x10-10	0.001	3.15	2.72	2.34

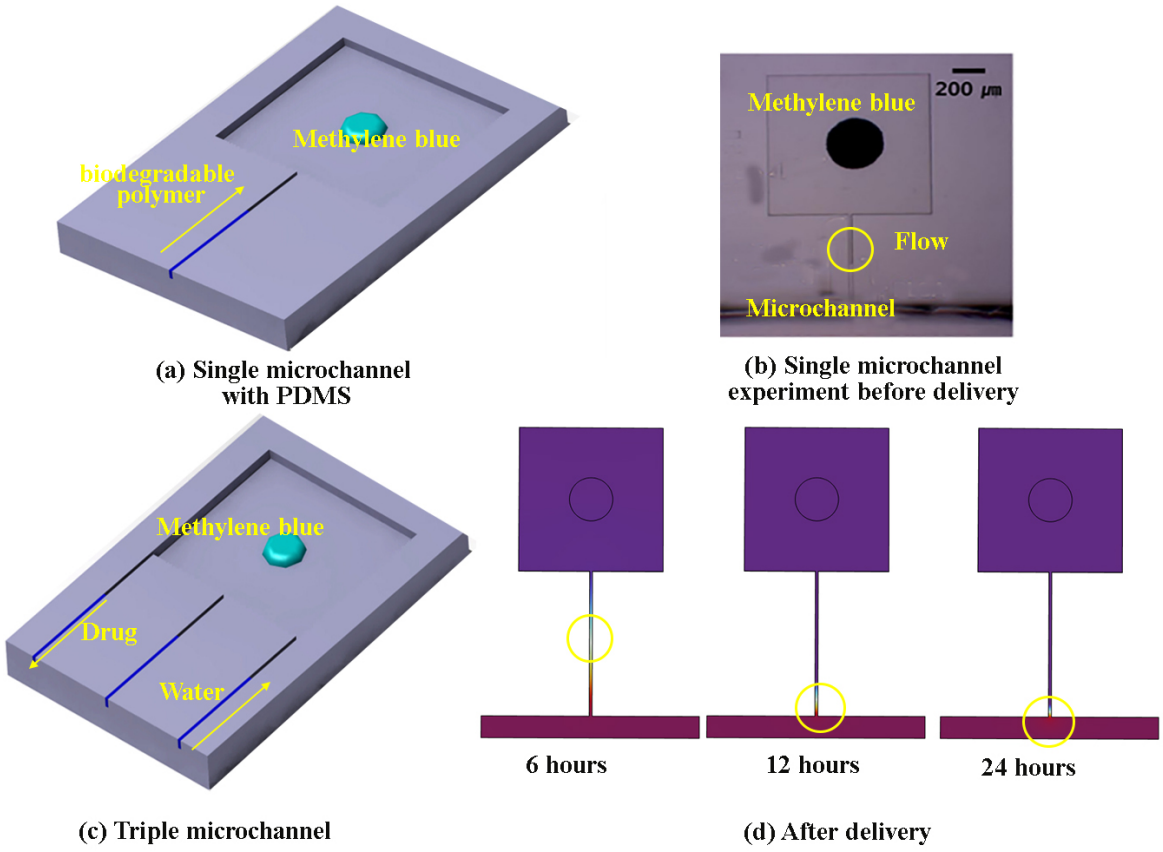

Fig. 12. Sequential delivery PDMS microchannel (a) Single straight channel (b) experiment setup (c) Triple microchannel (d) after delivery with PDMS setup.

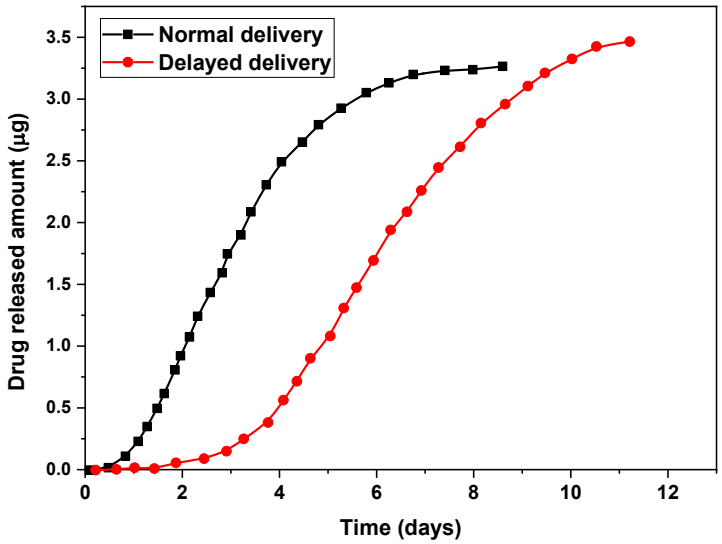

Fig. 13. Sequential drug delivery by PDMS degradable polymer using Methylene blue.

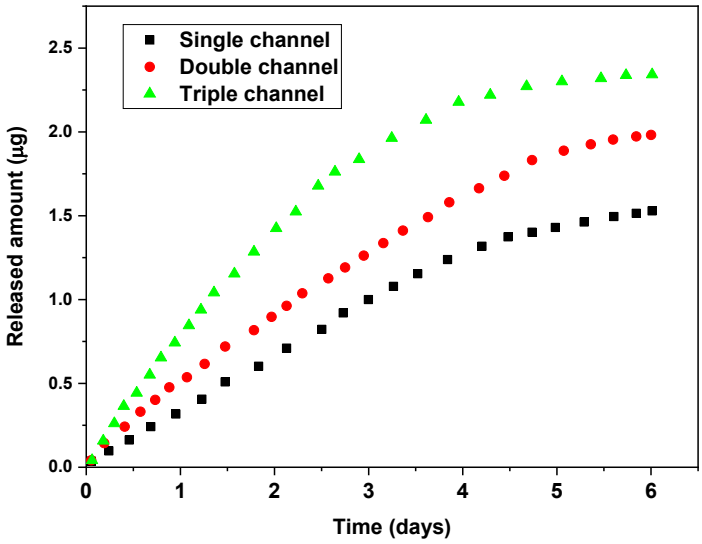

Fig. 14. Experimental results of released amount with single channel, double channel, triple channel.

3.4. Response Surface Methodology

3.4.1 Analysis of Variance (ANOVA)

The impacts of the variables that are influenced by one another, namely the A-Number of channels, B-Channel width, and C-Channel length, on drug release rate are displayed in ANOVA Table 6. The sufficiency of the models of regression was assessed according to the figures of the correlation coefficient (R2) and the adjusted determination coefficient (adj.-R2). The obtained R2 value 0.9940 implies a good fitting model and is well agreement with the numerical results. However, the inclusion of an independent variable into a model may yield a high R2 value, irrespective of the statistical significance of the added variable. Consequently, an adjusted R2 is commonly employed to achieve a more precise assessment of model suitability. Considering that all the models exhibited adjusted R2 values exceeding 0.8, it can be deduced that they closely correspond to the empirical data. The estimated coefficient of determination, denoted as R^2 with a value of 0.9940, exhibits a satisfactory level of concordance when compared to the adjusted coefficient of determination, denoted as R^2 with a value of 0.9873. This assertion is substantiated by the fact that the discrepancy between the two values does not exceed 0.2. The adequacy of the precision can be assessed by examining the adequacy ratio, which measures the relationship between the signal and the noise. An ideal scenario is characterized by a ratio that surpasses 4. In light of this, your ratio of 40.802 denotes a commendable level of signal adequacy.

Table 6 Effect of geometrical parameters on drug release rate (µg).

		Factor 1	Factor 2	Factor 3	Response 1	
Std	Run	A: Number of channels	B: Channel width	C: Channel length	Drug release rate	Predicted value
			µm	mm	µg	
7	1	1	5	3.4	1.23	1.14
8	2	3	5	3.4	3.45	3.40
13	3	2	5	1.65	2.48	2.47
1	4	1	2	1.65	0.62	0.67
5	5	1	5	0.7	1.02	1.05
9	6	2	2	0.7	2.25	2.14
2	7	3	2	1.65	3.06	3.00
15	8	2	5	1.65	2.48	2.47
3	9	1	20	1.65	0.94	0.95
12	10	2	20	3.4	2.45	2.47
10	11	2	20	0.7	2.18	2.15
16	12	2	5	1.65	2.48	2.47
18	13	2	5	1.65	2.48	2.47
14	14	2	5	1.65	2.48	2.47
4	15	3	20	1.65	2.95	2.94
11	16	2	2	3.4	2.05	2.17
17	17	2	5	1.65	2.41	2.47
6	18	3	5	0.7	3.21	3.32

Table 7. Analysis of variance for parameter evaluation.

Source	Sum of Squares	df	Mean Square	F-value	*p*-value	
Model	10.74	9	1.19	147.95	< 0.0001	significant
A-Number of channels	7.5	1	7.5	929.95	< 0.0001	
B-Channel width	0.0471	1	0.0471	5.84	0.042	
C-Channel length	0.0536	1	0.0536	6.65	0.0327	
AB	0.0354	1	0.0354	4.39	0.0695	
AC	0	1	0	0.0028	0.9594	
BC	0.0257	1	0.0257	3.19	0.1118	
A^2	0.3475	1	0.3475	43.08	0.0002	
B^2	0.3834	1	0.3834	47.54	0.0001	
C^2	0.0038	1	0.0038	0.4747	0.5103	
Residual	0.0645	8	0.0081			
Lack of Fit	0.0604	3	0.0201	24.67	0.002	significant
Pure Error	0.0041	5	0.0008			
Cor Total	10.8	17				

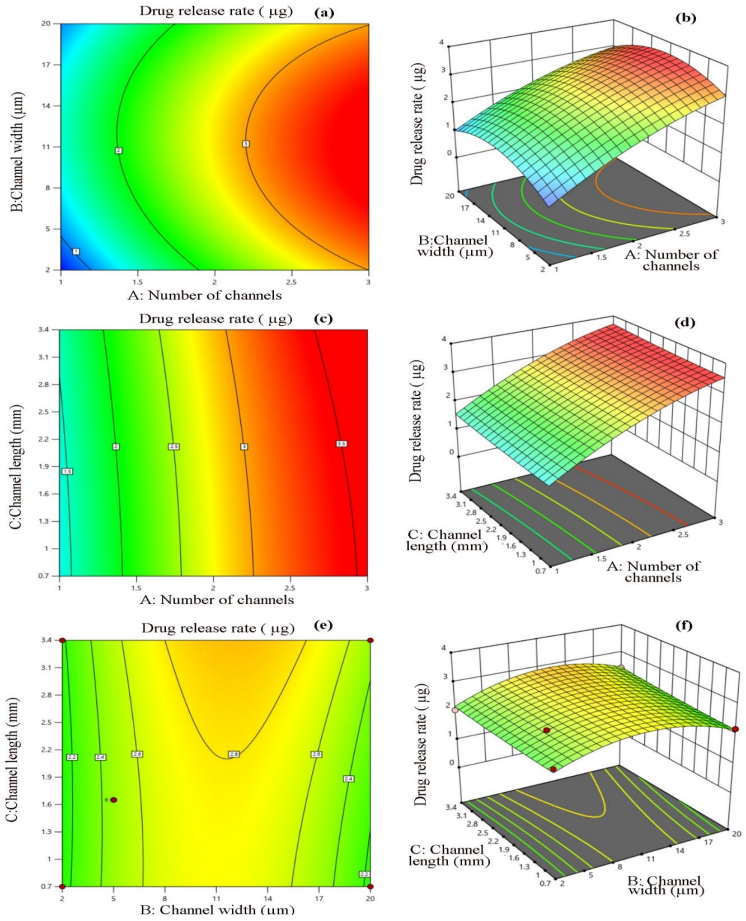

Fig. 15 (a-f). 3D and 2D contour surface showing effect of geometrical parameters interactions on drug release rate.

A *p* value is utilized in order to ascertain the statistical significance of a given model and its respective coefficient. The *p* values, being exceedingly low (<0.0001), indicate that the statistical analysis implies a high level of significance for the proposed model pertaining to each response (Table 7). The *p* value associated with lack of fit serves to determine whether a model adequately fits the data. Since the lack-of-fit values for all the fitted models were statistically significant ($p > 0.05$), it can be inferred that the proposed models are appropriate for the microchannel analysis.

3.6 Final Equation in Terms of Actual Factors

Drug release rate (µg/day) = -1.62236+2.32010*Number of channels+0.177161* Channel width-0.070154*Channel length-0.009490*Number of channels* Channel width-0.001715*Number of channels * Channel length+0.005869*Channel width * Channel length-0.283374*Number of channels ^{2}-0.007343*Channel width^2+0.018240*Channel length^2

When expressed in terms of tangible factors, the equation can be employed to generate prognostications concerning the reaction for specified magnitudes of all individual factors. In this case, the magnitudes must be explicitly denoted in the initial units for all factors. Applying this equation for determining each factor's relative influence is not recommended because the coefficients are adjusted to account for the units of each factor and the intercept needs to be positioned at the centre of the design space.

The visual representations of the interactions between the variables and their impacts on the responses are illustrated in Fig 15(a-f), using 2D contour plots and 3D response surface plots. It was determined how the independent variables affected the answers by looking at the linear, quadratic, and interaction terms in quadratic equations. An indicator that clarifies the impact of

variables on answers is a coefficient value. A higher value denotes a more significant impact. A positive value in the regression equation denotes an inverse link, whereas a negative value reflects a synergistic influence of factors on responses. The actual value is in good agreement with the predicted value, as shown in Fig. 16.

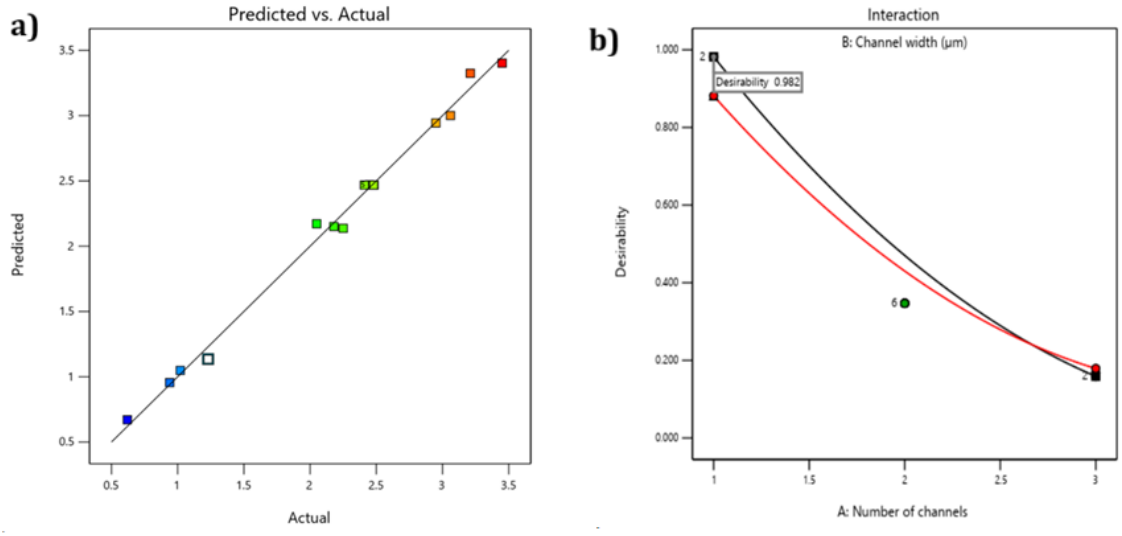

Fig. 16. Predicted Vs Actual.

4. Discussion

The aim of this study was to construct drug delivery systems that utilize microchannel technology, which enables precise calculation and regulation of the release rate by manipulating microchannel geometry. While many advances have been made in microfabricated drug delivery systems—more especially, reservoir-based systems—a thorough investigation into the use of discharge pathways has not been carried out [32]. the suggested formulation of medication compounds is discharged from the medication storage and advances towards the outer surface of the apparatus through a sequence of four distinct phases: 1) dissolution, 2) dispersion within the medication storage, 3) dispersion through the microfluidic channels. The introduction and systematic analysis of diffusion-based drug delivery have been presented [33]. In our study, the microfluidic systems were subjected to an application of an equivalent electrical circuit concept in order to enhance the intricate design and analysis.

Diffusion-based medication delivery has been introduced and analysed systematically [33]. In the present work, an analogous electrical system idea was used for microfluidic devices to improve their complex design and analysis. As indicated in Equation (1), it was projected that the augmentation of the diffusion flux would transpire in the case of broader and briefer conduits. The existence of numerous conduits can be understood as interconnected resistors, and correspondingly, the diffusion flux escalates alongside an increment in the quantity of conduits. Another fundamental constituent of an electrical circuit is known as a capacitor. Including a capacitor in an electrical circuit elongates the transition period until the capacitor reaches its maximum charge.

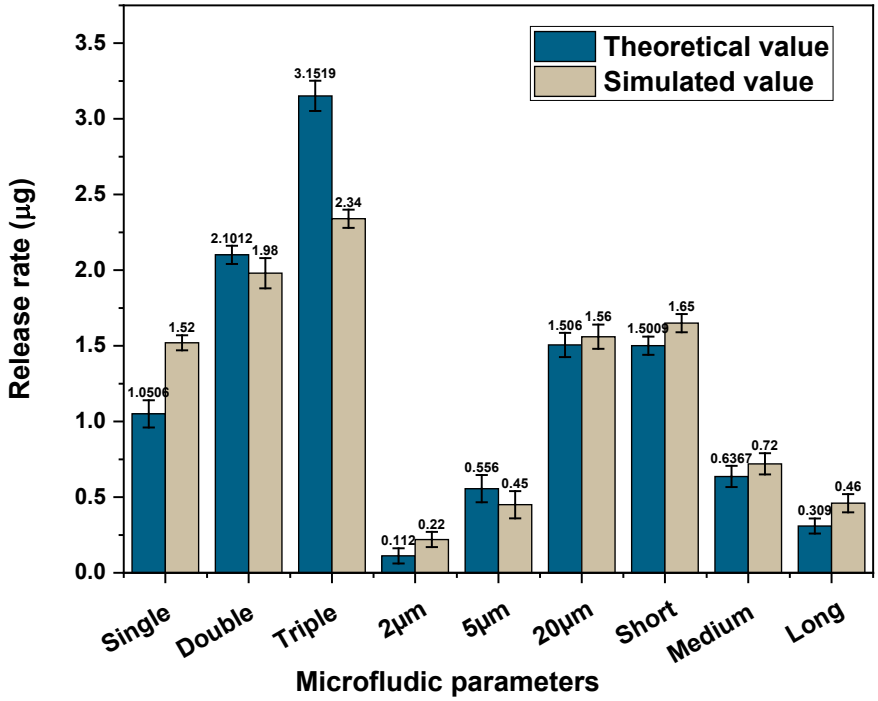

Fig.17 Release rate (µg) for different microfluidic parameters.

Similarly, we hypothesized that familiarizing a capacitor component with the microfluidic channel would protract the transient state. Due to the nature of Fick's first law, which delineates the transfer of mass in a state of equilibrium, it is not feasible to employ this law in forecasting the impact of capacitor integration on drug release behavior. Consequently, a Finite Element Method (FEM) simulation was performed to investigate the influence of capacitors on the system. It was observed that the simulated results and the in vitro test results showed a strong correlation with each other (as depicted in Fig. 18). Hence, it can be inferred that the duration of the transient state can be regulated by introducing capacitors into the system. The performance of drug delivery devices relies heavily on the precise management of the release initiation point, which is crucial for accurate scheduling. A time-dependent resistor as a biodegradable polymer was inserted into microfluidic channels. During the initial phase, the polymer exhibited an infinite resistance upon injection, effectively obstructing water infiltration into the drug reservoir and causing a delay in the entire delivery process. The capacitance of the channel structure changed from an infinite quantity to a value that was limited as the polymer deteriorated, allowing water to enter and aiding in the dispersion of medication molecules across the channels.

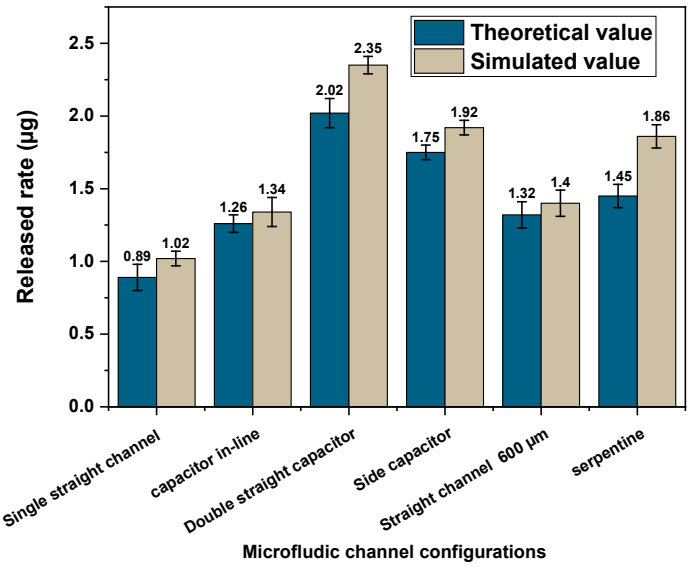

Fig. 18 Release rate (µg) for different microfluidic designs.

5. Conclusion

Microchannels played a crucial role as integral constituents of miniaturized fluid systems that relied on passive diffusion. These microchannels were effectively employed, for instance, to channel the flow of diffusing substances from the inlet to the outlet within a miniaturized PDMS device. A PDMS reservoir was selected due to its biocompatibility and its typical lack of reaction with the drug substance. Proposed PDMS channel architectures to administer medications in a precise and controlled manner. PDMS method involves modifying the channel shape to regulate the drug's delivery rate. Moreover, it demonstrated the effectiveness of multifunctional channel-based release devices that enable sequential drug release. The diffusion attribute of a microchannel was the outcome of dual effects. Initially, the drug's diffusion coefficient within a solution brought about a gap that was reliant on the concentration. From utilizing channel morphology to regulate the delivery rate, the investigation exhibited the efficacy of multifunctional release systems based on channels for sequential drug delivery. The ability to accomplish accurate yet convenient management of the release rate was realized by implementing diverse channel morphologies, as projected by finite element method-based modelling.

Availability of Data and Materials

All data analyzed during the study are included in this article and will be made upon reasonable request.

Author Contributions

T.A., performed conceptualization and methodology. N.N., performed data curation. S.P.K., performed writing- original draft preparation, reviewing and editing the manuscript. S.K supported for software and resources.

Acknowledgment

The author(s) received no financial support for the research, authorship, and/or publication of this article.

Funding

No funding obtained for this study.

Conflict of Interest

The authors declare no competing financial interest.

References

[1]. D. Huh, H. J. Choi, M. Byun, K. Kim, H. Lee, Long-term analysis of PV module with large-area patterned anti-reflective film, *Renewable* Energy **135**, 525-528 (2019); https://doi.org/10.1016/j.renene.2018.12.055

[2]. P. H. Krishnan, R. D. Sul, M. S. Murugan, V. Saravanan, Optimization of La and Ce mixed metal oxide hybrid for enhanced photoresponse in UV–Visible photosensing applications, *Journal of Materials Science: Materials in* Electronics **36**(22), 1377 (20250; https://doi.org/10.1007/s10854-025-15431-5

[3]. M. Dayanithy, G. C. Sekhar, R. C. Thivyarathi, P. Divyabharathi, L.P. Maguluri, V. Saravanan, Synergistic integration of $NiCo_2O_4$ and $NiWO_4$ nanosheets on Ni foam for advanced supercapacitor applications. *Journal of Porous Materials*, 1-11 (2025); https://doi.org/10.1007/s10934-025-01829-3

[4]. Z. Chen, J. B. Lee, Biocompatibility of su-8 and its biomedical device applications, Micromachines **12**(7), 794 (2021); https://doi.org/10.3390/mi12070794

[5]. K. H. Ke, C. K. Chung, High-performance Al/PDMS TENG with novel complex morphology of two-height microneedles array for high-sensitivity force-sensor and self-powered application, Small **16**(35), 2001209 (2020); https://doi.org/10.1002/smll.202001209

[6]. S. K. Sia, G. M. Whitesides, Microfluidic devices fabricated in poly (dimethylsiloxane) for biological studies, Electrophoresis **24** (21), 3563-3576 (2003); https://doi.org/10.1002/elps.200305584

[7]. J. Park, J. Li, A. Han, Micro-macro hybrid soft-lithography master (MMHSM) fabrication for lab-on-a-chip applications. *Biomedical* microdevices **12**(2), 345-351 (2010); https://doi.org/10.1007/s10544-009-9390-9

[8]. M. Pla-Roca, J. G. Fernandez, C. A. Mills, E. Martínez, J. Samitier, Micro/nanopatterning of proteins via contact printing using high aspect ratio PMMA stamps and nanoimprint apparatus Langmuir **23**(16), 8614-8618 (2007); https://doi.org/10.1021/la700572r

[9]. W. S. Lee, S. Jambovane, D. Kim, J. W. Hong, Predictive model on micro droplet generation through mechanical cutting, Microfluidics and nanofluidics **7**(3), 431-438 (2009); https://doi.org/10.1007/s10404-009-0412-y

[10]. P. S. Nunes, P. D. Ohlsson, O. Ordeig, J. P. Kutter, Cyclic olefin polymers: emerging materials for lab-on-a-chip applications. Microfluidics and nanofluidics **9**(2), 145-161 (2010); https://doi.org/10.1007/s10404-010-0605-4

[11]. E. Samiei, M. Hoorfar, Systematic analysis of geometrical based unequal droplet splitting in digital microfluidics, Journal of Micromechanics and Microengineering **25**(5), 055008 (2015); https://doi.org/10.1088/0960-1317/25/5/055008

[12]. K. A. Oliveira, P. B. M. e Silva, F. R. de Souza, F. T. Martins, W. K. T. Coltro. Kinetic study of glucose oxidase on microfluidic toner-based analytical devices for clinical diagnostics with image-based detection, Analytical Methods **6**(14), 4995-5000 (2014); https://doi.org/10.1039/c4ay00260a

[13]. J. Wang, L. Ren, L. Li, W. Liu, J. Zhou, W. Yu,... & S. Chen, Microfluidics: a new cosset for neurobiology. Lab on a Chip **9**(5), 644-652 (2009); https://doi.org/10.1039/b813495b

[14]. G. M. Whitesides, The origins and the future of microfluidics. nature **442**(7101), 368-373 (2006); https://doi.org/10.1038/nature05058

[15]. B. S. De, A. Singh, A. Elias, N. Khare, N, S. Basu, An electrochemical neutralization energy-assisted membrane-less microfluidic reactor for water electrolysis. Sustainable energy & fuels **4**(12), 6234-6244 (2020); https://doi.org/10.1039/d0se01474e

[16]. R. Liu, C. H. Chu, N. Wang, T. Ozkaya-Ahmadov, O. Civelekoglu, D. Lee,... & A.F. Sarioglu, Combinatorial immunophenotyping of cell populations with an electronic antibody microarray, Small **15(**51), 1904732 (2019); https://doi.org/10.1002/smll.201970275

[17]. A. Vasudev, A. Kaushik, K. Jones, S. Bhansali, Prospects of low temperature co-fired ceramic (LTCC) based microfluidic systems for point-of-care biosensing and environmental sensing, Microfluidics and nanofluidics **14**(3), 683-702 (2013); https://doi.org/10.1007/s10404-012-1087-3

[18]. A. Chango, L. Abdennebi-Najar, F. Tessier, S. Ferré, S. Do, J.L. Guéant, F. Willequet, Quantitative methylation-sensitive arbitrarily primed PCR method to determine differential genomic DNA methylation in Down Syndrome, Biochemical and biophysical research communications **349**(2), 492-496 (2006); https://doi.org/10.1016/j.bbrc.2006.08.038

[19]. P. Serrano, D. Decanini, L. Leroy, L. Couraud, G. Hwang, Multiflagella artificial bacteria for robust microfluidic propulsion and multimodal micromanipulation. Microelectronic Engineering **195**, 145-152 (2018); https://doi.org/10.1016/j.mee.2018.04.003

[20]. S. Soheili, E. Mandegar, F. Moradikhah, M. Doosti-Telgerd, H.A. Javar, Experimental and numerical studies on microfluidic preparation and engineering of chitosan nanoparticles, Journal of Drug Delivery Science and Technology **61**, 102268 (2021); https://doi.org/10.1016/j.jddst.2020.102268

[21]. L. Zhang, Q. Chen, Y. Ma, J. Sun, Microfluidic methods for fabrication and engineering of nanoparticle drug delivery systems. ACS Applied Bio Materials **3**(1), 107-120 (2019); https://doi.org/10.1021/acsabm.9b00853

[22]. G. Shim, M. G. Kim, D. Kim, J. Y. Park, Y. K. Oh, Nanoformulation-based sequential combination cancer therapy, Advanced drug delivery reviews **115**, 57-81 (2017); https://doi.org/10.1016/j.addr.2017.04.003

[23]. Y. Huang, S. S. Venkatraman, F. Y. Boey, E. M. Lahti, P. R. Umashankar, M. Mohanty, S. Vaishnav, In vitro and in vivo performance of a dual drug-eluting stent (DDES), Biomaterials **31**(15), 4382-4391 (2010); https://doi.org/10.1016/j.biomaterials.2010.01.147

[24]. T. A. Holland, Y. Tabata, A. G. Mikos, Dual growth factor delivery from degradable oligo (poly (ethylene glycol) fumarate) hydrogel scaffolds for cartilage tissue engineering, Journal of Controlled Release, **101**(1-3), 111-125 (2005); https://doi.org/10.1016/j.jconrel.2004.07.004

[25]. D. B. Pacardo, F. S. Ligler, Z. Gu, Programmable nanomedicine: synergistic and sequential drug delivery systems, Nanoscale **7**(8), 3381-3391 (2015); https://doi.org/10.1039/c4nr07677j

[26]. D. Sengeni, R. Nadanasabai, V. Saravanan, L. Sangeetha, J. U. Prakash, Development of binary transition metallic selenide (NiSe/Co3Se4) hybrid counter electrode for highly efficient Pt-free dye-sensitized solar cells, Ionics **30**(12), 8281-8293 (2024); https://doi.org/10.1007/s11581-024-05871-0

[27]. P. Byass, The global burden of liver disease: a challenge for methods and for public health, BMC medicine **12**(1), 159 (2014); https://doi.org/10.1186/s12916-014-0159-5

[28]. V. Arunprasad, P. Rapur, D. Hemanand, M. A. Bennet, V. Saravanan, Design and fabrication of nanoarchitectures of rGO-decorated ZnCo2O4 hybrid photocatalyst for high-efficiency solar fuel generation, Journal of Materials Science: Materials in Electronics **36** (3), 192 (2025); https://doi.org/10.1007/s10854-025-14285-1

[29]. V. Saravanan, M. Arthy, S. A. Jayakar, S. Suganya, T. Archana, M. Thirumalai, Hierarchical $ZnCo_2O_4/MoS_2$@ rGO nanocomposite on nickel foam: a promising electrode for advanced energy storage, Ionics **31** 1-13 (2025); https://doi.org/10.1007/s11581-025-06399-7.

[30]. S.S. Nath, K. Chanthirasekaran, S.S. Priya, N. Bharathirja, D. Gupta, S. Kumaran, Boosting electrochemical behavior of biomass-derived porous carbon via N, S, and N, S co-doping for enhanced supercapacitor performance, Diamond and Related Materials 112850 (2025); https://doi.org/10.1016/j.diamond.2025.112850

[31]. K. Prabhu chandran, S. S. Nath, K. Sudha, T. Vinod Kumar, S. Kumaran, J. Sasidevi, Strategic Design of TiO2-SnS Hybrid Nanostructures: Dual-Function Catalysts for Antibiotic Removal and Solar Energy Conversion in DSSCs, Journal of Electronic Materials 1-17 (2025); https://doi.org/10.1007/s11664-025-12377-6

[32]. M. Syamala, D. Srivastava, S.D. Khandekar, T. Porselvi, M.K. Patan, A. Balaram, S. Kumaran, Construction of g-C3N4 anchored Cu-ZnS hybrid nanostructures for sustainable energy storage and environmental remediation, Research on Chemical Intermediates **51** 1-30 (2025); https://doi.org/10.1007/s11164-025-05713-2

[33]. J. Siepmann, F. Siepmann, Modeling of diffusion controlled drug delivery. Journal of controlled release **161**(2), 351-362 (2012); https://doi.org/10.1016/j.jconrel.2011.10.006